

Wideband millimeter wave absorber based on coding-metasurface with two-dimensional MXene

Kevin Brower^{a,*}, Brendan DeLacy^b, Benjamin Garrett^b, and Mark Mirotznik^a

^aUniversity of Delaware, Electrical and Computer Engineering Department, Newark, Delaware, United States

^bBallydell Technologies, Inc., Wilmington, Delaware, United States

ABSTRACT. This study investigated MXene ink as the absorbing material in a wideband millimeter wave (MMW), metasurface absorber and applied the ink in a periodic array. The MXene ink was characterized in the Ka-band, and a Debye permittivity model was found that accurately described the highly frequency-dependent properties. A 1-bit coding-metasurface algorithm was used to discover an optimized design that minimized the average reflectance at normal incidence, utilizing the unique properties of the materials. The absorber was fabricated using hybrid processing techniques and measured at multiple incident angles to compare against the simulated design. The absorber demonstrated a wideband response (i.e., 14 GHz bandwidth) at normal incidence with a greater than 93% absorptance from 26 GHz to 40 GHz and an average reflectance of 2% over the entire band. Furthermore, the absorber tested at a 10-deg incident angle demonstrated a greater than 91% absorptance at the Ka-band and an average reflectance of 3.4% across the band; Tested at a 20-deg incident angle, the absorber demonstrated a greater than 88.5% absorptance and an average reflectance of 3.9% across the band. The study established the value of using MXene ink in metasurface absorbers for wideband applications in MMW frequencies.

© The Authors. Published by SPIE under a Creative Commons Attribution 4.0 International License. Distribution or reproduction of this work in whole or in part requires full attribution of the original publication, including its DOI. [DOI: [10.1117/1.OE.63.2.027105](https://doi.org/10.1117/1.OE.63.2.027105)]

Keywords: millimeter wave; metamaterial; coding-metasurface; absorber; MXene; electromagnetics

Paper 20230924G received Sep. 29, 2023; revised Jan. 25, 2024; accepted Jan. 29, 2024; published Feb. 20, 2024.

1 Introduction

Traditional electromagnetic (EM) absorbers generally fall into resonant or broadband classes. Resonant structures offer high absorbing properties but typically only operate efficiently in narrow frequency bands. Broadband absorbers, such as pyramidal foam absorbers and graded absorbers, offer wideband properties at the cost of increased weight and thickness. Over the last decade, several advances have been made in the design of EM absorbers intended to overcome the limitations of traditional approaches. One is a class of EM absorbers that leverages recent advances in metamaterials.¹ Metamaterials are engineered materials, typically consisting of periodic arrays of sub-wavelength patterns with unique EM properties. Metamaterial-based absorbers (MMA) overcome the limitations of traditional absorbers² by exploiting novel designs and tailored material properties, allowing for enhanced absorption characteristics, wideband performance, and even tunability.³ A large amount of literature has been published on designing MMAs that operate from a few GHz to visible light frequencies.^{4,5}

*Address all correspondence to Kevin Brower, kcbrower@udel.edu

A second emerging area is using two-dimensional (2D) materials for EM shields and absorbers. Two-dimensional materials, such as graphene, graphene oxides, and MXenes, possess extraordinary EM properties attributed to their high carrier mobilities, large surface areas, and low mass density. Of the various 2D material families, the MXenes have demonstrated some of the most interesting electrical properties. MXenes are a relatively new family of two-dimensional layered transitional metal carbides, nitrides, or carbonitrides that exhibit a variety of unique characteristics.⁶ MXenes originate from $M_{n+1}AX_n$ (or MAX) phases, which are formed by a stack of successive atomic layers of transition metals (M), elements from groups 13 to 15 of the periodic table (A), and carbon or nitrogen (X). The A layers are less strongly bonded than the others and can be removed. As a result, the MX layers are separated from one another and form what are called MXenes. Ti_3C_2 is the most well-studied MXene. An essential characteristic of MXene composition is the surface termination functional groups produced by the electrochemical etching fabrication method. The interface termination units also impact the electrical and ion transport characteristics of MXenes and, hence, its electrical conductivity. MXenes have been explored for various technology applications, but many developmental efforts have focused on their use in energy storage systems, EM interference (EMI) shielding, and water purification.⁷

In this research, we combined MXene ink with a coding metamaterial-based design approach to realize thin millimeter wave absorbers that possess high absorption efficiencies (>93%) over a wide frequency band (26 to 40 GHz) and range of incident angles. Specifically, our approach is to pattern a thin MXene layer deposited onto the surface of a grounded dielectric substrate. Our device architecture, illustrated in Fig. 1, assumes a periodic pattern of 2D unit cells, each which are divided into a 10×10 array of pixels and coded with ones (MXene) or zeros (no MXene) demonstrating a coding-metasurface optimization approach.⁸ To the best of our knowledge, this is the first study to combine a patterned custom-synthesized MXene coating with MMA design codes to develop wideband absorbers. Table 1 presents some related research illustrating this paper's unique aspects.

The outline for the subsequent portion of the paper is as follows. Section 2 presents the development and EM characterization of the materials used to create the MMAs, including the MXene inks. Section 3 describes the 1-bit coding metasurface design algorithm, including several design examples. The methods used to fabricate and conduct metrology on experimental samples are described in Sec. 4. In Sec. 5, the experimental characterization system is used

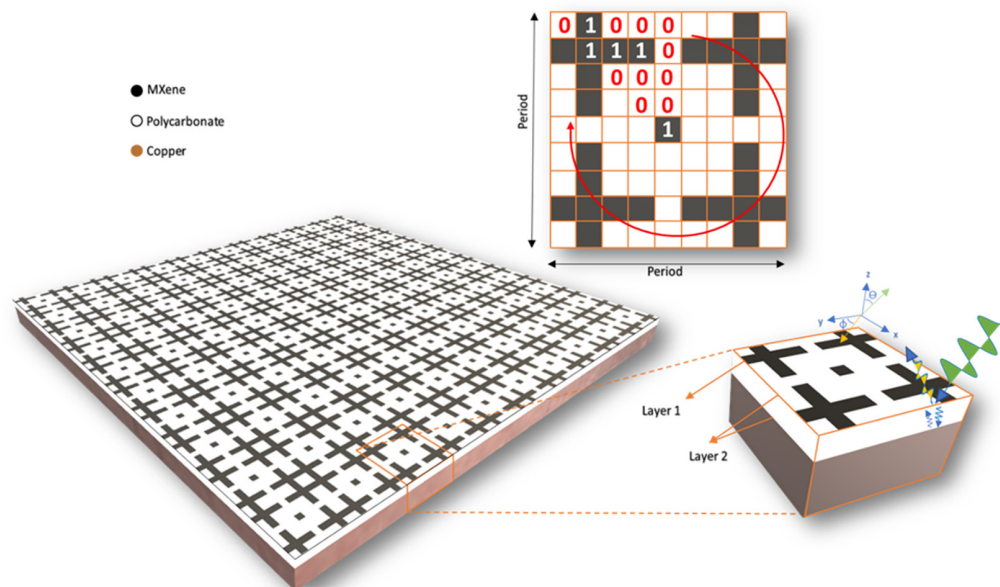


Fig. 1 (left) 3D representation of fabricated periodic array sample; (right) unit cell depicting EM wave interaction of three-layer system each; and (top) 2D illustration of a 1-bit coding-metasurface design with 1s representing MXene and 0s representing air.

Table 1 A snapshot of other comparable studies.

Study	Design method	Absorbing material	Frequency range (GHz)	Application
Zheng et al. ⁹	Coding-metasurface	Graphene	40 to 60	Beam steering
Chen et al. ¹⁰	Characteristic modes analysis	Silver	1 to 7	Wideband absorption
Xin et al. ¹¹	Known SRR structures	Copper	20 to 44	Wideband absorption
Ullah et al. ¹²	Known SRR structures	MXene	3 to 5	EMI shielding (design only)
Li et al. ¹³	Salisbury screen	Indium tin oxide	4.1 to 17.5	Wideband absorption
This work	1-bit coding metasurface	MXene	26 to 40	Wideband absorption

to measure our devices' wideband absorption properties and give experimental results. The final section discusses the primary results and suggests future research.

2 Materials and Characterization

2.1 Ti₃C₂ MXene Synthesis

Ti₃C₂ MXene was first synthesized using the mixed acid method previously described in the literature.¹⁴ Briefly, 2 mL HF (50%, Acros Chemical), 12 mL HCl (36% to 38%, Fisher Chemical), and 6 mL water were added to a polypropylene bottle and magnetically stirred. Next, 1 g of Ti₃AlC₂ powder (Millipore Sigma, 910775) was slowly added to the mixture, stirring at 300 RPM and 35°C. The mixture was stirred for 24 h. The solution was then placed in a centrifuge at 3500 RPM for 5 min. The supernatant was subsequently decanted into a suitable waste container. Water was then added to the remaining sediment, and the contents were shaken well by hand. The centrifugation and washing steps were repeated until the supernatant exhibited a neutral pH. The remaining sediment, a mixture of multilayered and monolayered MXene, was resuspended in water and placed in a centrifuge for 1 h at 3500 RPM. The resulting dark supernatant, consisting of mono and few-layered MXene, was collected and placed in a separate collection bottle. Water was added to the sediment remaining in the centrifuge tube, the contents were shaken well by hand, and the mixture was again placed in a centrifuge for 15 min at 3500 RPM. The washing and centrifugation steps of the sediment were repeated until the supernatant became clear. The sediment left behind in the centrifuge tube consisted of multilayered MXene and was discarded. Finally, the monolayered and few-layered MXene was stored in the collection bottle and was further concentrated via centrifugation at 10,000 RPM for 10 min. In this final step, the clear supernatant was removed, and the MXene sediment was resuspended in a suitable volume of water to achieve the desired concentration. The final MXene suspension was then mixed with a proprietary binder to form a sprayable MXene formulation (Ballydel Technologies, product #MX001).

2.2 Electromagnetic Characterization

The coding-metasurface technique necessitates a comprehensive understanding of the material properties of the MXene ink to develop an accurate model for wideband optimization. Although measuring the properties of freestanding MXene layers can be challenging, their characterization becomes feasible when the properties of the substrate to which the MXene adheres are known. To this end, we employed a free-space focused beam method to characterize the complex permittivity of the MXene coatings applied to a polycarbonate substrate. The 3D printed substrate was 1.27 mm thick and had a measured permittivity of 2.65. It is observed that the measured dielectric permittivity of the substrate deviates from conventional values,^{15,16} ranging from 2.75 to 2.85, due to the presence of air pockets caused by the 3D printing process, resulting in an effective permittivity. The uniform layer of MXene ink was deposited on the polycarbonate substrate with a measured average thickness of 3.1 μm. The sample was placed in the center of a free-space focused beam system, as depicted in Fig. 2, and the transmission and reflection coefficients were measured from 18 to 40 GHz. A standard transfer matrix method¹⁷ was used to determine the

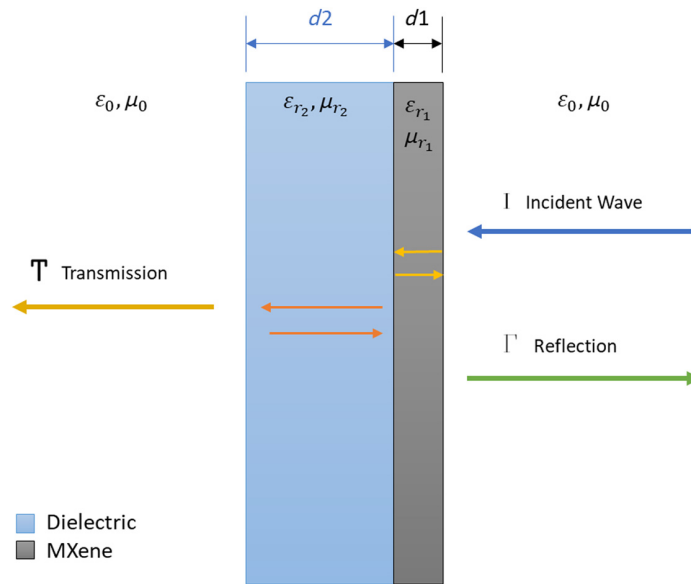


Fig. 2 Two-layered dielectric slab with known $d1$ and $d2$ thicknesses, transmission and reflection coefficients, and substrate permittivity used to calculate MXene complex permittivity.

permittivity through the two-layered dielectric sample by using the known thicknesses, the permittivity of the substrate, and the transmission through the slab. The unknown frequency-dependent complex permittivity of the MXene layer was then determined by varying its complex permittivity computationally until the simulated transmission and reflection coefficients matched the measured values.

The sheet resistance (R_s) of the layer composed of MXene and polyurethane can be adjusted to achieve optimal performance of the metamaterial absorber. R_s is defined by the expression

$$R_s = \frac{1}{\sigma * t} \left[\frac{\Omega}{sq.} \right], \quad (1)$$

where σ represents the conductivity of the material, and t is the thickness of the layer. The lossy properties of the material are explained by the complex relative permittivity values, given as

$$\epsilon_r = \epsilon' - j * \epsilon'', \quad (2)$$

where ϵ'' is the conduction loss factor describing the relationship between frequency and conductivity

$$\epsilon'' = \frac{\sigma}{\omega * \epsilon_0}. \quad (3)$$

We conducted a sweep of full-wave simulations where the sheet resistance of the absorbing layer was varied over a wide range. It was found that a sheet-resistance in the range of 100 Ω /sq. resulted in metasurface designs with a high level of absorption over the frequency band of interest. Additionally, it was found experimentally using our selected deposition method that a print thickness of $\sim 3 \mu\text{m}$ resulted in consistent and uniform deposition of ink on the substrate. Based on these results, the complex permittivity of the MXene/polyurethane composite was tuned to achieve the desired sheet-resistance by varying the mass percent of polyurethane in the ink formulation for our desired print thickness of (Fig. 3).

The complex permittivity properties of MXene ink were measured and are depicted in Fig. 3. The data was fit to a standard Debye dispersion model,¹⁸ represented as follows:

$$\epsilon_{\text{MXene}}(f) = \epsilon_\infty + \frac{\epsilon_s - \epsilon_\infty}{1 + j2\pi f \cdot \tau}. \quad (4)$$

The following values were obtained from the Eq. (4) and later incorporated into the design of the metasurface: $\epsilon_s = 7,503.6$, $\epsilon_\infty = 924.9$, and $\tau = 12.71$ pico-seconds.

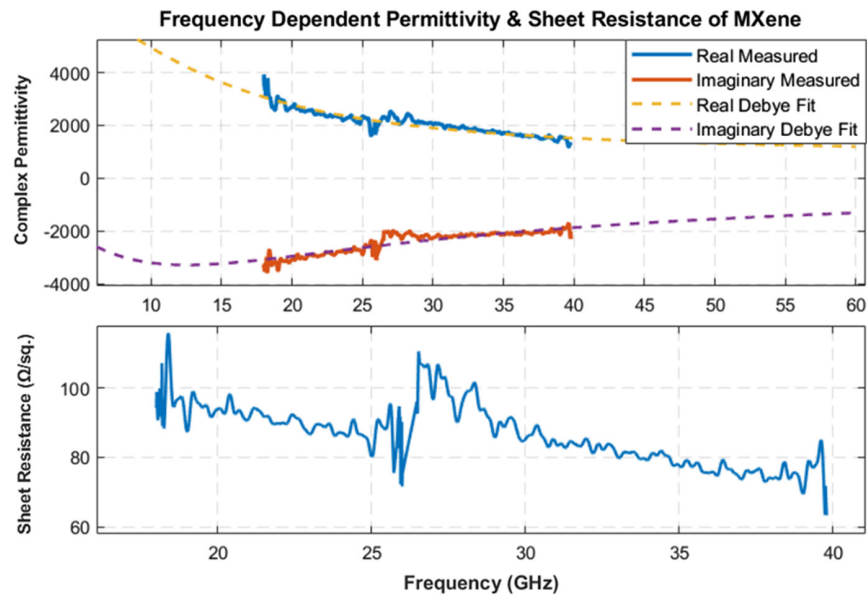


Fig. 3 Measured complex permittivity of MXene ink fit to a Debye dispersion model from 18 to 40 GHz.

3 Coding-Metasurface Design

3.1 Optimization Algorithm

An iterative optimization algorithm was developed to synthesize the unit cell pattern of the MXene metasurface absorber. This design approach relies on the previously measured complex permittivity properties of the MXene ink in addition to the thickness and substrate properties. While a wide variety of metasurface patterns could be used, we employed the 1-bit coding-metasurface technique. In this method, each unit cell is divided into a 2D array of smaller square “pixels” that either contain MXene or do not. This approach is commonly referred to as a one-bit coding metasurface due to each pixel either having (i.e., “1”) or not having (i.e., “0”) conductive material. This binary coding system provides a convenient structure for iterative optimization approaches, such as genetic algorithms or particle swarm optimization (PSO). A similar design approach has been used in other studies, such as Ramachandran et al.¹⁹ to create multiple narrowband absorption peaks, Mourad et al.²⁰ to reduce the radar cross section of a perfect electric conductor plate, or Zheng et al.⁹ to design a reconfigurable millimeter wave (MMW) antenna.

It should be noted that a direct search algorithm for the optimal unit cell pattern would require an impractical number of computational resources. For example, the unit cell used in this study, composed of a simple 10×10 array of “pixels,” contains 2^{100} possible patterns. Thus, a more intelligent approach that leverages the various symmetries is necessary. To this end, we further sectioned the unit cell into eight quadrants, as shown in Fig. 1. We imposed mirror symmetries along the horizontal, vertical, and diagonal axes denoted in the figure. This reduced the number of unknowns by approximately a factor of eight and reduced the number of possible patterns by a very substantial amount ($\sim 2^{(N/8)}$). We then employed the iterative optimization algorithm shown in Fig. 4. Here, the user first defines the incident field conditions (i.e., frequency band, incident angles, and polarization states), substrate and MXene properties (i.e., layer thicknesses and permittivities), and unit cell dimensions (i.e., period and the number of pixels in both the x and y directions). For most absorber designs, the substrate thickness is chosen to be one-quarter of the material wavelength at the center of the frequency band of interest. The unit cell period is generally preferred to be small enough such that only the zeroth diffractive order propagates at the highest frequency (i.e., shortest wavelength) but not too small such that the smallest features (i.e., pixels) become too difficult to fabricate.

The iterative algorithm begins with a random set of metasurface patterns, analyzed over the desired incident field conditions using a full-wave EM solver. While several solvers could be used for this purpose, we found that the rigorous coupled wave method (RCW) produced

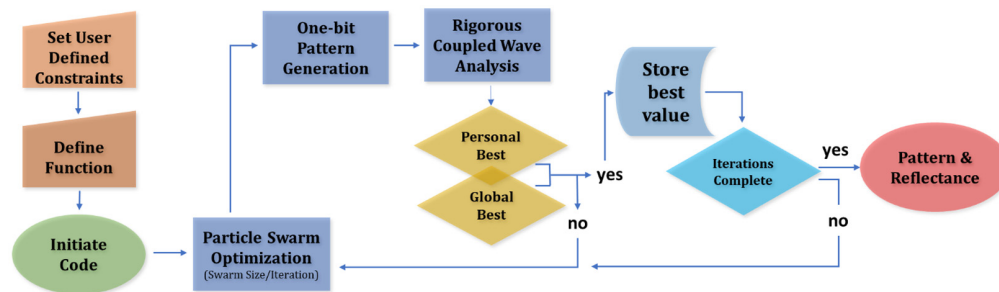


Fig. 4 Flowchart for the metasurface optimization process. After user constraints and objective function is defined, the PSO iterative process begins until the global minimum is found.

accurate results with the lowest computational expense. The RCW method is well-known in the photonics community for providing efficient full-wave solutions of periodic layered surfaces. Our specific custom implementation of RCW followed the approach described in a study by Lalanne and Morris²¹ and returned reflectance results, $R(f, \theta)$, from each test pattern over the range of frequencies and incident angles of interest. A single metric, or objective function, was then calculated as a means of quantifying what is considered an improved result. For our wideband absorber application, we used the objective function given in Eq. (5), which attempts to minimize the average reflectance over the range of illumination conditions

$$F = \min(\text{avg.}(R(f, \theta))). \quad (5)$$

The PSO method is then used to intelligently vary the coding metasurface pattern until either the algorithm has converged or the user stops the algorithm after an acceptable result is found.

3.2 Design Examples

To assess the effectiveness of MXene as an absorbing metasurface material, a series of optimization simulations was performed within the K and Ka frequency bands (18 GHz to 40 GHz), utilizing the previously described algorithm. Three distinct design simulations were conducted, each imposing unique period and frequency band constraints while maintaining key parameters, such as MXene sheet thickness ($3.1 \mu\text{m}$), MXene permittivity (as detailed earlier), substrate thickness (1.27 mm), and substrate dielectric constant (2.65). These simulations were devised to identify MXene-based geometric patterns capable of minimizing the average reflectance at normal incidence. Demonstrating MXene's potential to absorb EM energy across multiple frequency bands effectively, Fig. 5 presents an overview of the designs, and average reflectance results catering to wide and narrowband applications.

The first simulation targeted narrowband performance at 2 GHz bandwidth, utilizing a 4.5 mm period to minimize the reflectance from 21 to 23 GHz. The optimization process yielded an average reflectance of 0.7% in the specified frequency window and is plotted in Fig. 6 from 18 to 40 GHz, highlighting its designed bandwidth as a solid line and illustrating narrowband absorptance. In contrast, the second simulation focused on wideband performance within the K-band (18 to 26 GHz) utilizing a period of 5 mm, resulting in an average reflectance of

Name	Pattern	Avg. Reflectance (%)	Period	Designed for
Narrow Band		0.7	4.5 mm	Narrowband from 21 – 23 GHz
K Band		2.3	5 mm	Wideband from 18 – 26 GHz (k-band)
Ka Band		2.4	6 mm	Wideband from 26 – 40 GHz (ka-band)

Fig. 5 Optimized design examples using MXene as absorbing metasurface material.

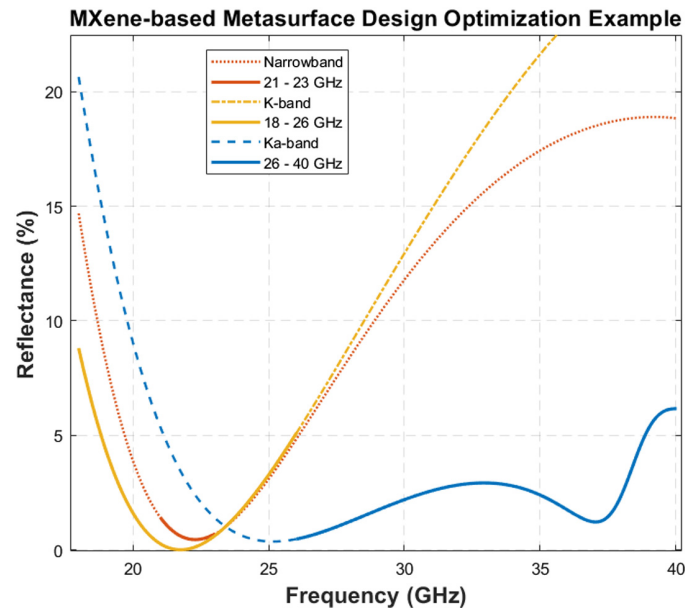


Fig. 6 Reflectance of optimized metasurface design examples using different constraints, including varying periods and frequency bands. The metasurfaces were optimized for frequency bands indicated in the legend.

2.3% across this band. Finally, the third simulation again aimed to optimize wideband performance, targeting the Ka frequency band (26 to 40 GHz) instead. This design used a period of 6 mm and yielded an average reflectance of 2.4% across the entire frequency band. The third metasurface example, showcasing wideband performance in the Ka-band, was selected for fabrication to validate the model's accuracy due to its superior performance, larger bandwidth, and utilization of the higher frequency, MMW band.

4 Hybrid Fabrication

4.1 Hybrid Processing

The design method and simulation results for the optimized metamaterial absorber are realized through fabrication using hybrid, additive, and subtractive techniques to provide greater options in the design concerning substrate availability and reduction of material processing cost and time. The substrate was created using a multi-tool platform that allowed the 3D printing of the polycarbonate feedstock using fused filament fabrication and a micro-milling tool to smooth the top surface to the desired thickness. The substrate was then provided to Ballydel, Inc., who deposited the MXene ink using a standard model airbrush kit to coat the surface in the same way as was done in the characterization steps, attempting to control the thickness of the ink as much as possible. The absorber was placed in a laser etching/engraving system with a 420 mm lens attachment, and the unit cell design was imported into the software to create the periodic array, applying the previously tested and determined etching parameters (power, frequency, and speed). The laser etching process took approximately 15 min for the 4" × 4" (101.6 mm × 101.6 mm) surface to fully etch the periodic array, resulting in an entire fabrication time of around 4 h. A copper ground plane was then attached to the underside of the absorber with commercial adhesive spray.

4.2 Metrology

Measurements of the dimensions with respect to each fabrication process were performed to identify the accuracy of the actual feature sizes compared to the design, informing the performance results gained from the EM measurements in the next section. With respect to the substrate thickness, eight measurements across the surface were taken [Fig. 7(a)] using a coating thickness gauge accurate to 1.0 μm . It was found that the substrate thickness varied from 1.21 to 1.31 mm with a mean value of 1.24 mm. This represents only a 2% average deviation from the desired substrate thickness of 1.27 mm.

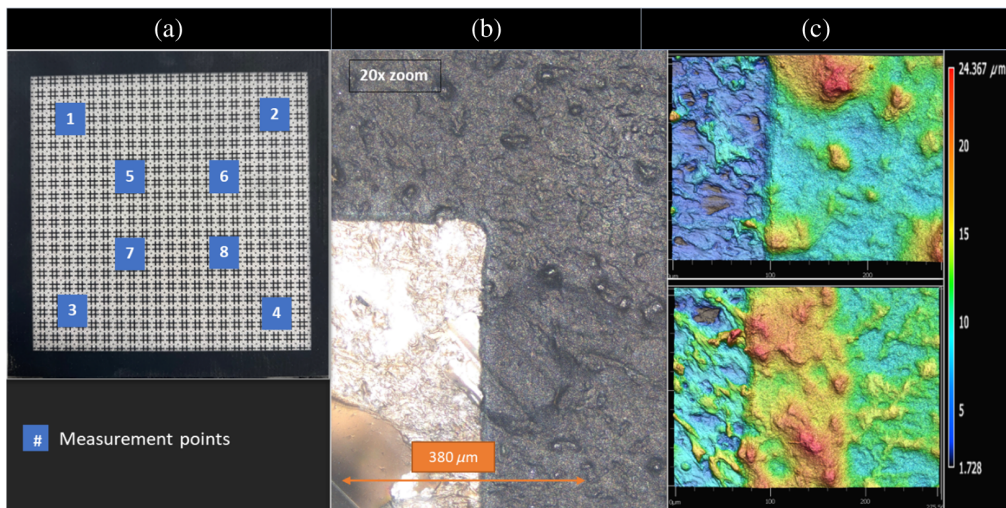


Fig. 7 (a) Final fabricated absorber consisting of periodic MXene elements. (b) 20× zoom image of the interface between etched MXene ink and substrate. (c) Color map images were taken using a laser confocal microscope, showing the etched interface indicating deformation and peaks.

The thickness of the MXene ink is a critical parameter that determines the optimal absorbing performance of the features, and Fig. 7(b) shows a 20× zoom image of a portion of the unit cell, shows some visual flaws associated with pitting and edge issues with MXene deposition (black portion). Laser measurements were taken using the Keyence VK-X series microscope to characterize the laser-etched MXene geometries. Figure 7(c) shows color map images of two different post-etched elements of the boundaries between the substrate and MXene ink, where greater thickness is indicated by the brighter colors (yellow/red). The average variation of the thickness of ink was measured over five different elements across the surface, and while the thicknesses ranged from 1.9 to 6.7 μm, the average thickness was calculated to be 3.6 μm. As demonstrated later in this manuscript this variation in ink thickness likely had a measurable impact on the overall device performance.

The dimensions of the metamaterial unit cell geometry could potentially affect the frequency-dependent absorption results if they differ from the design dimensions. Figure 8 shows the results of side-by-side measurements that were again taken using the Keyence confocal microscope. Each of the 11 measurements was taken 3 separate times on different unit cells over the surface of the etched metasurface to characterize the variation of the etching method. Figure 8 lists the averages of each of those measurements and the calculated average percent error based on the actual dimensions of the design. The table shows that the most significant percent error of any of the measurements is less than 8%, and the lowest is 0.14%. The laser etching method of patterning proved to be fairly consistent over the test samples with little variation between measurements; however, some of the more significant discrepancies could affect the magnitude of absorption.

5 Design Verification, Results, and Discussion

5.1 Testing Methods

The EM performance for the fabricated MXene-based metamaterial absorber was performed using two distinct methodologies: (1) a focused beam measurement system and (2) an NRL arch. The focus beam measurement system, illustrated in Fig. 9(a), employed a Gaussian beam to evaluate the absorber's response under normal incidence from 18 to 40 GHz. In contrast, the custom-designed NRL Arch [Fig. 9(b)] facilitated bistatic measurements, enabling an assessment of the absorber's effectiveness across varying incident angles from 26 to 40 GHz. The arch was constructed with a semi-circular curvature and brackets positioned at 10-deg intervals from the center. The EM characteristics were analyzed through the evaluation of transmission, reflection, and absorption components, with their cumulative sum equating to unity. Furthermore, the incorporation of a copper-backed absorber rendered the transmission component negligible.

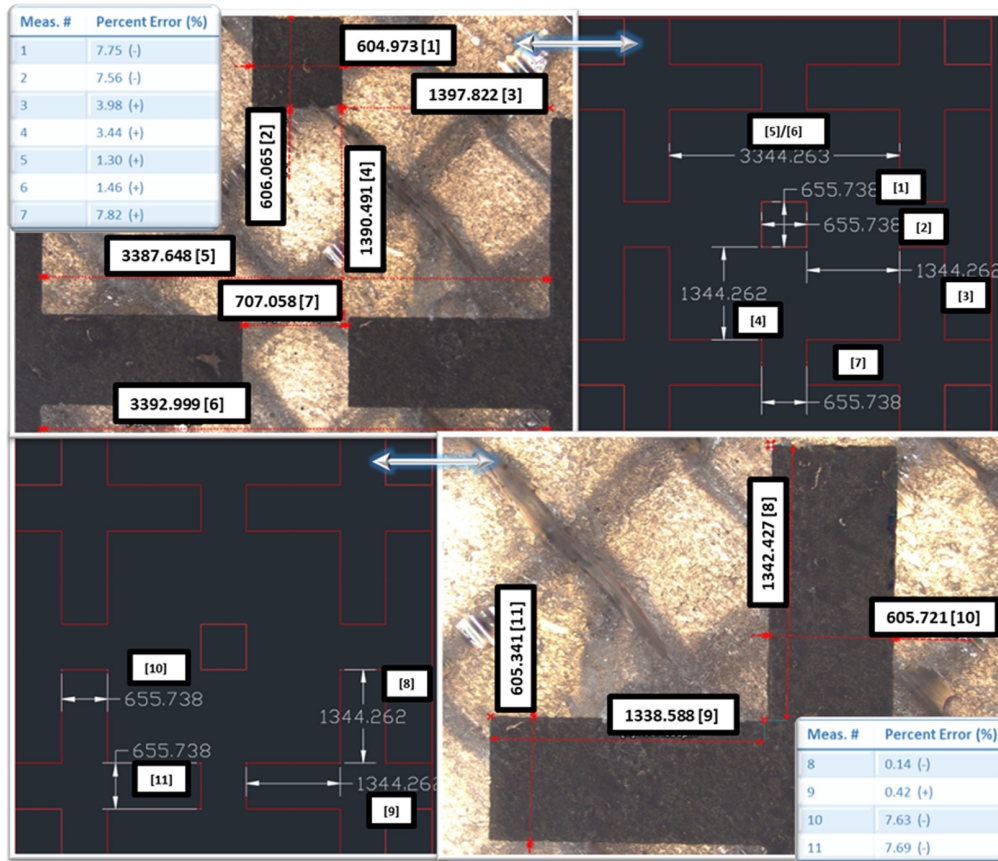


Fig. 8 Confocal imaging of metasurface features showing measured dimensions next to designed values. Error values are presented in percent as either larger than (+) or smaller than (-), the design dimensions.

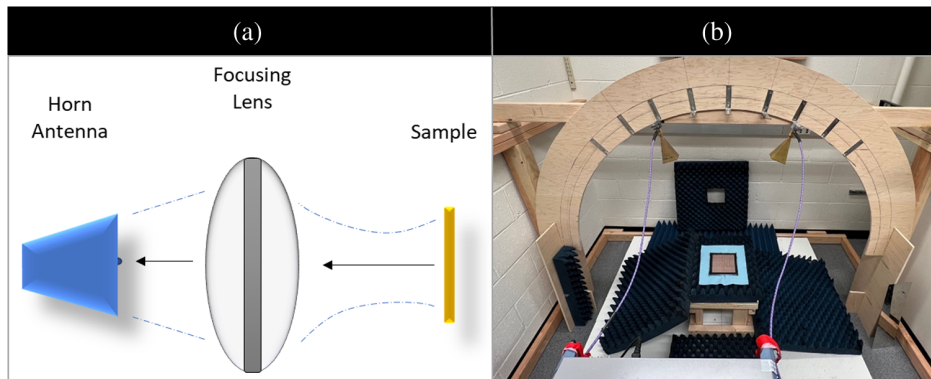


Fig. 9 Testing methods used in the study: (a) a monostatic, focus beam measurement system converging a Gaussian beam on a sample at normal incidence and reflecting energy back to the horn antenna. (b) NRL arch measurement platform with testing available at 10-deg increments from the center.

The reflectance of the absorber, expressed as a percentage, was determined by quantifying the reflection coefficient and subsequently calculated.

5.2 Measurement Results and Discussion

The reflectance measurements were conducted with the focus beam system at normal incidence across the frequency range of 18 to 40 GHz and juxtaposed against the simulated design spanning 18 to 44 GHz, as depicted in Fig. 10. Within the targeted Ka-band (26 to 40 GHz), where the

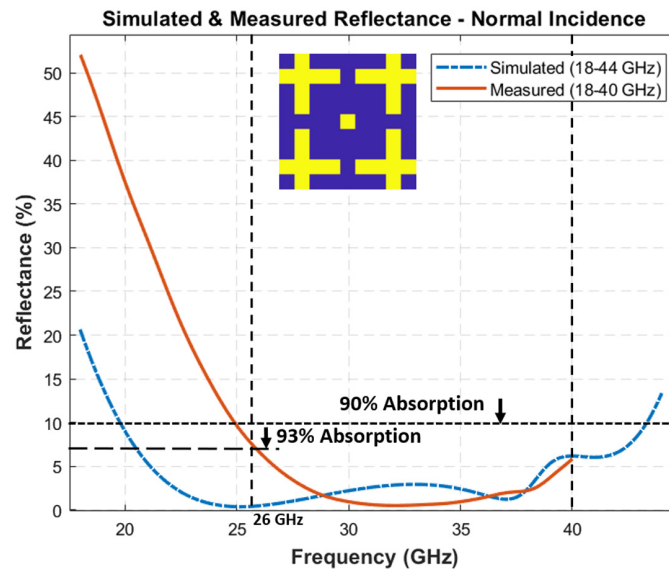


Fig. 10 Reflectance given in percent of the simulated design metasurface and the measured results demonstrating a greater than 93% absorptance at normal incidence in the Ka-band.

metasurface optimization was focused, an absorptance exceeding 93% was observed. Across this band, the calculated average reflectance remained at a low value of 2%. This performance was consistent with the simulation-derived value of 2.4% average reflectance in the Ka-band. Notably, the fabricated absorber exhibited a broad-spectrum absorptance in the frequency ranges of 25 to 40 GHz, encompassing over 90% absorptance over a 15 GHz bandwidth. Evident in this analysis is the strong agreement between the simulated accuracy of the coding-metasurface model and the realized performance of the fabricated absorber. This coherence was particularly pronounced within the band of 27 to 40 GHz, where the reflectance alignment lay within a $\pm 3.5\%$ range. The experimental results thus validate the model's predictive capabilities while affirming the absorber's proficiency in attaining desired absorptance and reflectance characteristics in the design band. However, the discrepancies outside the design band (< 26 GHz) prompted further evaluation that will be addressed later in the text.

The absorber's evaluation encompassed varying incident angles, utilizing both the simulated RCWA method and the fabricated metasurface via the NRL Arch. The presented measurements at a 10-deg angle shown in Fig. 11, similar to the normal incidence graph, revealed good

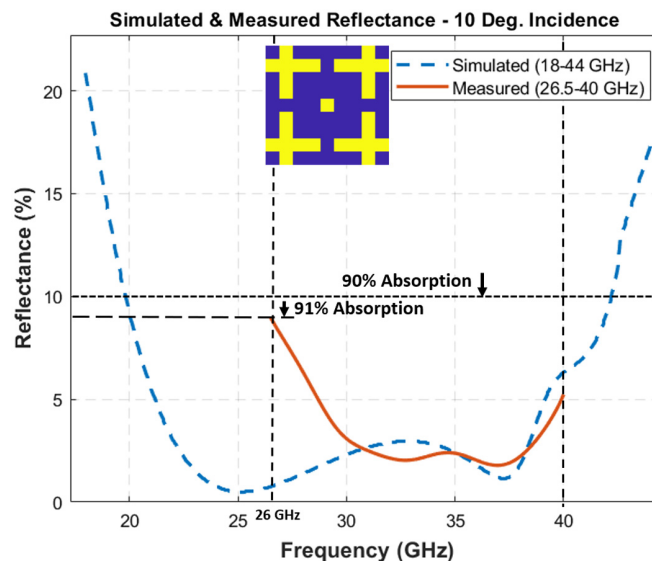


Fig. 11 Measured and simulated design reflectance results over the Ka-band at a 10-deg incident angle.

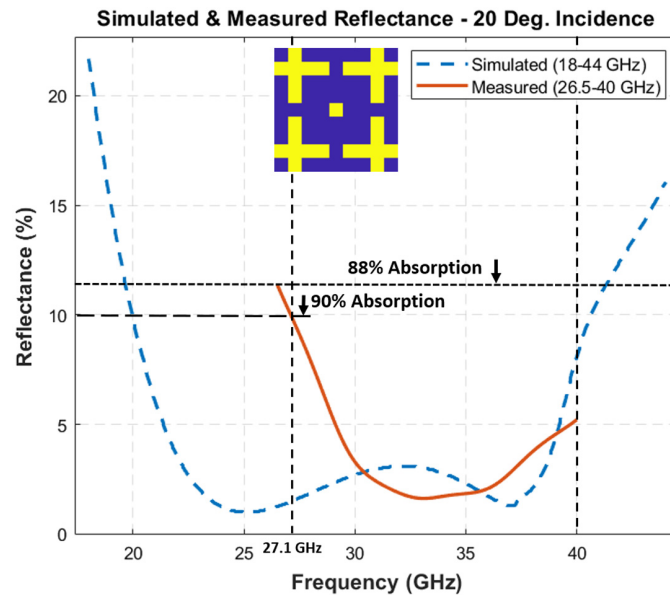


Fig. 12 Measured and simulated design reflectance results over the Ka-band at a 20-deg incident angle.

performance even at slight angles, demonstrating absorptance exceeding 91%. The computed results returned a 3.4% average reflectance over the entire band, slightly deviating from the simulated average reflectance of 2.4%. Within the frequency range of 29 to 40 GHz, the reflectance difference between measured and simulated results remained below 2.6%. However, at lower frequencies, a notable elevation in reflectance difference, ranging from 2.6% to 8.2%, emerged between model and measured values from 26.5 to 29 GHz. These results highlight the absorber's consistent performance under varied angles and offer insights into the frequency-dependent discrepancies for future analysis and refinement.

Using the NRL Arch, measurements were conducted employing horn antennas situated at 20-degree angles from the center, with both measured and simulated results depicted in Fig. 12. As anticipated, the absorber's performance declined at this elevated angle; nevertheless, it produced an absorptance exceeding 90% from 27.1 to 40 GHz and an average reflectance of 3.9% within the 26.5 to 40 GHz range. This is similarly compared to a simulated average reflectance of 2.6%. Notably, the most substantial deviations were observed at lower frequencies, with reflectance differences between simulated and measured values ranging approximately from 3% to 10% spanning 29 to 26.5 GHz while remaining below 3% reflectance difference from 29 to 40 GHz. This analysis emphasizes the absorber's wideband performance despite the pronounced increase in reflectance at the lower frequency range.

The design process successfully identified a metasurface geometry that effectively lowered reflectance within the Ka-band and was subsequently validated through fabrication. Nevertheless, discrepancies between the simulated and measured outcomes prompted further investigation. To better understand the underlying cause of this discrepancy, we conducted additional simulations based on the metrology data extracted from the fabricated device.

The reduced x and y -dimension feature sizes identified in the metrology results were applied in the initial simulation. The outcomes demonstrated an increase in reflectance by up to 7% compared to the simulated curve, thereby aligning more closely with the measured results, as observed in Fig. 13. Subsequently, the second simulation incorporated metrology thickness measurements that revealed a minimum MXene thickness value of $1.9 \mu\text{m}$. Again, the outcome demonstrated an increase in reflectance focused in the lower frequencies of up to a 24% increase compared to the original simulated curve. The final simulation encompassed both width feature size adjustments and thickness modifications depicted in Fig. 13, incorporating the simulated metrology results. This approach yielded a reflectance difference of less than 4% between the resulting simulation and the measured fabricated results across the majority of the frequency band. These findings underscore two significant observations: first, while all three dimensions

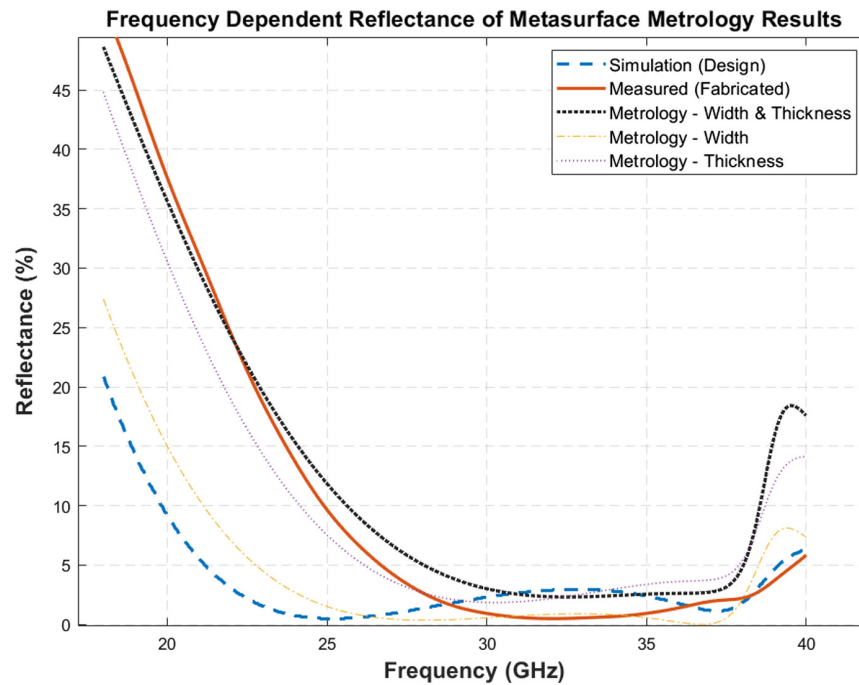


Fig. 13 Alternate simulations based on metrology results of fabricated metasurface showing the adjusted dimensions more closely matching measured results.

of the MXene ink metasurface features notably influence reflectance errors in the fabricated absorber, the thickness dominates the resulting simulation and measurement disagreements; secondly, the coding-metasurface and RWCA modeling is successful in harnessing MXene's distinct properties for the creation of effective metasurfaces.

6 Conclusion and Future Work

This study demonstrated that 2D materials, such as MXene inks, used as the absorbing layer within a metasurface absorber can be an effective method for realizing wide-band EM absorption within the microwave and MMW bands. By capitalizing on the distinct frequency-dependent material properties of MXene inks combined with an iterative optimization algorithm, unit cell geometries were found that minimized reflectance over a wide frequency band. The practicality of our approach was demonstrated by several simulation examples and experimentally validated for one of those examples. The fabricated MXene-based absorber exhibited wideband absorption exceeding 93% at normal incidence, over 91% at 10 deg, and above 88.5% at 20 deg over all frequencies from 26 to 40 GHz. The metasurface absorber validated the optimization goal by demonstrating an average reflectance of 2% at normal incidence, 3.5% at 10 deg, and 3.9% at 20 deg in the Ka-band, highlighting the effectiveness of MXene ink as an absorbing material.

There are several areas to improve these results further. One improvement would be to better characterize and optimize the laser etching process to control the dimensional accuracy of fabricated features. Another alternate option would be to design for the shrinking features by adding the expected dimensional loss to the digital design elements to decrease the impact of the fabricated device. Another fabrication variation could be to alter the deposition method to a technique such as screen-printing to better control the consistency of MXene ink over the surface, which was identified as an issue. This could also lead to the development of a roll-to-roll fabrication process for large surface area applications.

Furthermore, while the performance of the 1-bit coding metasurface and RCWA techniques to develop an optimized MXene-based metasurface was proven to be successful, some methods can be implemented to expand design opportunities. The design process could be improved by introducing additional geometrical features (e.g., split rings). Finally, our approach could be applied to a multiple-layered absorber, allowing for enhanced wide-band performance.

Disclosures

There are no potential conflicts of interest, financial or otherwise, identified for this study.

Code and Data Availability

The data that support the findings of this article can be requested from the author at kcbrower@udel.edu

Acknowledgments

There are no acknowledgements to make. Any funding for project was internal to the university.

References

1. S. Ramya and I. Srinivasa Rao, "An ultra-thin compact wideband metamaterial absorber," *Radioengineering* **27**(2), 364–372 (2018).
2. R. C. Jain, "Understanding electromagnetic wave absorbers," *IETE J. Educ.* **41**(1–2), 35–43 (2000).
3. R. M. H. Bilal et al., "Tunable and multiple plasmon-induced transparency in a metasurface comprised of silver S-shaped resonator and rectangular strip," *IEEE Photonics J.* **12**(3), 1–13 (2020).
4. S. Narayan and A. Kesavan, Eds., *Handbook of Metamaterial-Derived Frequency Selective Surfaces*, Metamaterials Science and Technology, Springer Nature, Singapore (2020).
5. R. Anwar, L. Mao, and H. Ning, "Frequency selective surfaces: a review," *Appl. Sci.* **8**(9), 1689 (2018).
6. M. Naguib et al., "25th anniversary article: MXenes: a new family of two-dimensional materials," *Adv. Mater.* **26**(7), 992–1005 (2013).
7. M. Naguib, M. W. Barsoum, and Y. Gogotsi, "Ten years of progress in the synthesis and development of MXenes," *Adv. Mater.* **33**(39), 2103393 (2021).
8. T. J. Cui et al., "Coding metamaterials, digital metamaterials and programmable metamaterials," *Light: Sci. Appl.* **3**(10), e218 (2014).
9. B. Zheng et al., "Multiple-beam steering using graphene-based coding metasurfaces," *Micromachines* **14**(5), 1018 (2023).
10. H. Chen et al., "Design and experimental validation of a low-profile wideband metamaterial absorber by characteristic modes analysis," *Results Phys.* **28**, 104684 (2021).
11. W. Xin et al., "Design and characterization of an ultrabroadband metamaterial microwave absorber," *IEEE Photonics J.* **9**(3), 1–13 (2017).
12. Z. Ullah, M. A. Hasan, and I. Ben Mabrouk, "EMI shielding for 5G IOT devices with MXene metamaterial absorber," in *9th Int. Conf. Internet of Things: Syst., Manage. and Secur. (IOTSMS)*, IEEE (2022).
13. T. Li et al., "Optically transparent metasurface Salisbury screen with wideband microwave absorption," *Opt. Express* **26**(26), 34384 (2018).
14. M. Anayee et al., "Role of acid mixtures etching on the surface chemistry and sodium ion storage in Ti3C2Tx MXene," *Chem. Commun.* **56**(45), 6090–6093 (2020).
15. B. Salski et al., "Complex permittivity of common dielectrics in 20–110 GHz frequency range measured with a Fabry–Pérot open resonator," *Appl. Phys. Lett.* **119**(5), 052902 (2021).
16. H.-Y. Yao, D.-R. Hsiao, and T.-H. Chang, "Fast, nondestructive, and broadband dielectric characterization for polymer sheets," *Polymers* **12**(9), 1891 (2020).
17. S. J. Orfanidis, "Multilayer structures," Chap. 6 in *Electromagnetic Waves and Antennas*, pp. 186–227, Rutgers University (2016).
18. I. Zivkovic and A. Murk, "Free-space transmission method for the characterization of dielectric and magnetic materials at microwave frequencies," in *Microwave Materials Characterization*, InTechOpen (2012).
19. T. Ramachandran and M. R. I. Faruque, "Impact of compact and novel 1-Bit coding based metamaterial design for microwave absorption applications," *J. Magn. Magn. Mater.* **563**, 170044 (2022).
20. A. Mourad, L. Burgnies, and E. Lheurette, "RCS reduction by 1-bit coding metasurface," in *IEEE Conf. Antenna Meas. & Appl. (CAMA)*, IEEE (2021).
21. P. Lalanne, "Improved formulation of the coupled-wave method for two-dimensional gratings," *J. Opt. Soc. Am. A* **14**(7), 1592 (1997).

Kevin Brower is currently pursuing his PhD in electrical engineering at the University of Delaware with a focus in electromagnetics and optics. He previously received his BS degree in energy engineering from Penn State University in State College, Pennsylvania, United States. His research focus is on design, characterization, and fabrication of wideband and electromagnetic absorbers. Other related research interests include advanced manufacturing methods for electronics, optics, and electromagnetic applications.

Brendan DeLacy is president and founder of Ballydel Technologies. His technical interests include the synthesis and characterization of novel nanomaterials and composites, as well as the optimization of the electromagnetic, thermal, mechanical, and electronic properties of these materials. He received his BS and MS degrees in chemistry from St. Joseph's University, a MS degree in applied physics from Johns Hopkins University, and a PhD in analytical chemistry from Drexel University.

Benjamin Garrett is a PhD in electrical engineering working with Ballydel Technologies, Inc. in Wilmington, Delaware. He received his degree in 2021 from the University of Delaware where he focused on microparticle approaches for optical and infrared scattering applications, 3D printing of reconfigurable antennas, and several electromagnetic-related projects. His primary focus with Ballydel is on 2D materials synthesis and applications, optical holography applications, RF imaging technologies, and more.

Mark Mirotznik received his BSEE degree from Bradley University, Peoria, Illinois, United States and his MSEE and PhD degrees from the University of Pennsylvania, Philadelphia. Currently, he is a professor in the Department of Electrical and Computer Engineering and the associate dean for Research and Entrepreneurship for the College of Engineering at the University of Delaware, in Newark, Delaware, United States. His research interests include applied electromagnetics and photonics, computational electromagnetics, multifunctional engineered materials, and additive manufacturing.